

Quench dynamics of the $2d$ XY model

Asja Jelić¹ and Leticia F. Cugliandolo²

¹Université Paris-Sud, Laboratoire de Physique Théorique, CNRS UMR 8627,

Bâtiment 210, Orsay F-91405, France

²Université Pierre et Marie Curie - Paris 6,

Laboratoire de Physique Théorique et Hautes Energies, CNRS UMR 7589,

4, Place Jussieu, Tour 13, 5ème étage, 75252 Paris Cedex 05, France

February 16, 2022

Abstract

We investigate the out of equilibrium dynamics of the two-dimensional XY model when cooled across the Berezinskii-Kosterlitz-Thouless (BKT) phase transition using different protocols. We focus on the evolution of the growing correlation length and the density of topological defects (vortices). By using Monte Carlo simulations we first determine the time and temperature dependence of the growing correlation length after an infinitely rapid quench from above the transition temperature to the quasi-long range order region. The functional form is consistent with a logarithmic correction to the diffusive law and it serves to validate dynamic scaling in this problem. This analysis clarifies the different dynamic roles played by bound and free vortices. We then revisit the Kibble-Zurek mechanism in thermal phase transitions in which the disordered state is plagued with topological defects. We provide a theory of quenching rate dependence in systems with the BKT-type transition that goes beyond the equilibrium scaling arguments. Finally, we discuss the implications of our results to a host of physical systems with vortex excitations including planar ferromagnets and liquid crystals as well as the Ginzburg-Landau approach to bidimensional freely decaying turbulence.

1 Introduction

The out of equilibrium dynamics of systems with continuous symmetries annealed or quenched from the symmetric to the symmetry broken phase are a subject of study in different branches of physics. Liquid-crystals quenched across a phase transition into their ordered phase present a large variety of topological defects that diffuse, interact and eventually annihilate [1]. Vector ferromagnets cooled across their Curie temperature are other condensed-matter examples with a variety of dynamic topological defects [2]. Cosmology provides a set of interesting models in which similar dynamics occur [3]. Still, the decay

of vortex density in freely decaying turbulence has also been of interest [4]. In all these areas, there is considerable interest in the dynamics of defects once the phase transition has been crossed.

Of special interest is the planar time-dependent Ginzburg Landau model with $SO(2)$ symmetry or its lattice counterpart the $2d$ XY model. A static phase transition occurs at a finite critical temperature, T_{KT} , between a high- T disordered paramagnet and a low- T ferromagnetic phase with quasi-long range order. When the model is quenched from the high to the low temperature phase the continuous symmetry of the disordered phase is broken to the one of the ordered phase. In these systems the defects are singular vortices that carry topological charge and have logarithmic interactions. In the high- T phase free vortices proliferate while in the low- T phase vortices bind in pairs. Physical realizations are bidimensional planar ferromagnets [2], superconducting films [5], Josephson-junction arrays [6], especially tailored nematic liquid crystals [7], and toy models for bidimensional turbulence [4]. The exponential singularity may also describe the critical properties of superfluid helium films [8].

Phase ordering kinetics following an infinitely rapid quench through a thermal critical point have been extensively studied in the statistical physics literature [9]. In condensed matter applications the time spent close to the critical point is typically much shorter than the time spent far from it and, therefore, the infinitely fast quench approximation is justified. A few studies where cooling rate dependencies have been taken into account are [10, 11, 12, 13]. The study of cooling-rate dependencies in defect dynamics is, instead, central in cosmology. The goal in this case is to estimate the density of defects, ρ , left over in the universe after it went through a number of potential (second-order) phase transitions. The importance lies on the fact that, initially, these were thought to act as seeds for matter clustering. This scenario seems to be excluded by observation data now but, still, the interest in predicting the density of topological defects remains due to other possible effects of these objects [14]. In the late 80s Zurek derived a quantitative prediction for ρ that is based on critical scaling in the disordered phase close to a second order phase transition. The proposal is based upon the hypothesis whereby the defect dynamics should be negligible below the transition. In consequence, ρ is assumed to remain fixed to the value it takes at the control parameter at which the system falls out of equilibrium in the disordered phase. In his articles Zurek proposed to check these predictions in condensed matter systems with the same symmetry properties as the cosmological models [15]. A vast experimental [16, 17] and numerical [18] activity followed with variable results summarized in [19].

The fact that the annihilation of defects can be neglected in the out of equilibrium regime was questioned in [20]. In this paper, a scaling argument that includes the mechanism of defect annihilation in the low-temperature phase for systems with second-order phase transitions and dissipative dynamics was proposed. A scaling of the density of defects with cooling rate *and* time spent in the out of equilibrium evolution was derived. The predictions were checked numerically with Monte Carlo dynamics of the $2d$ Ising model, a paradigmatic system with discrete symmetry breaking. Similar ideas about the importance

of the dynamics below the transition were stressed in [21].

The treatment of all cases mentioned in the previous paragraph is classical. Recently, pushed by the advent of powerful experimental techniques in cold atom systems, the extension of the Kibble-Zurek mechanism to quantum *isolated* systems was developed [22, 23, 24]. These claims have been critically revisited in [25, 26], as reviewed in [27].

In this paper we examine the density of vortices left over after going through the Berezinskii-Kosterlitz-Thouless classical phase transition [28, 29] with a finite speed. We revisit the Kibble-Zurek mechanism and we provide a theory of quenching rate dependence in systems with continuous symmetry and the BKT-type of ‘infinite-order’ phase transition that goes beyond the equilibrium scaling arguments. We test it with a Monte Carlo numerical study of the $2d$ XY model on a square lattice. We work in the canonical setting, in the sense that the system is coupled to an equilibrium environment that allows for energy dissipation. As a control parameter driving the phase transition we use the temperature of the heat-bath. For concreteness we use linear cooling procedures, characterized by a single parameter, the cooling rate. A previous numerical study of this problem with a different method that ignores the effects of free-vortices appeared in [30]. We shall discuss the results in this paper and confront them to ours in the body of this work.

The organization of the paper is the following. In Sect. 2 we recall the definitions of the $2d$ XY model and the time-dependent Ginzburg-Landau equation and we present the Monte Carlo method used. In Sect. 3 we shortly review the BKT scenario. Section 4 is devoted to the analysis of infinitely rapid quenches. In Sect. 5 we present our results on annealing procedures. Finally, in Sect. 6 we give our conclusions.

2 Model and method

In this section we recall the definition of the $2d$ XY model and we describe the Monte Carlo method that we use in our simulations of the lattice model. We also explain the corresponding time-dependent Ginzburg-Landau stochastic equation.

2.1 The $2d$ XY model

The two-dimensional XY model is defined by the Hamiltonian

$$H = -J \sum_{\langle i,j \rangle} \vec{s}_i \cdot \vec{s}_j, \quad (1)$$

with ferromagnetic exchange coupling, $J > 0$. The spins are classical variables constrained to live on a plane. $\vec{s}_i^2 = 1$, and the sum runs over nearest neighbours on a square lattice of linear size L . It is convenient to use a parametrization in which the spin vector is represented by the angle it forms with a chosen axis,

$\vec{s}_i = e^{i\theta_i}$; with it the Hamiltonian becomes

$$H = -J \sum_{\langle i,j \rangle} \cos(\theta_i - \theta_j) . \quad (2)$$

Above the critical temperature T_{KT} , unbound positively and negatively charged vortices are present and the system is disordered. Below T_{KT} vortex-antivortex pairs bind and the system is critical in a sense that we shall make more precise below. The critical temperature is found to be $k_B T_{KT} \simeq 0.89J$ [29]. We measure T in units of J/k_B in the following.

2.2 Dynamics

Stochastic dynamics, mimicking the coupling of the classical spins to a thermal bath, can be attributed in different ways. In this Section we define the Monte Carlo procedure used in our simulations. We focus on non-conserved order-parameter dynamics (model A) in which the magnetization is not conserved. We also briefly recall the time-dependent Ginzburg-Landau approach.

2.2.1 Monte Carlo dynamics

We performed a Monte Carlo study of the $2d$ XY model on a square lattice of linear size L with periodic boundary conditions. The Monte Carlo algorithm consists in updating the angular variable θ_i associated to a randomly chosen site i to a new value θ'_i randomly chosen in the interval $[-\pi, \pi]$, with probability $p = \min\{1, e^{-\beta\Delta E}\}$, where ΔE is the energy variation between the two configurations. Equilibrium data are for relatively small system sizes, $L = 16$ to $L = 50$, while out of equilibrium ones are for larger samples, $L = 100$ to $L = 400$. We briefly discuss finite size effects when presenting the simulation data. The results are an average of 5 to 10000 independent runs each (depending on the quantity calculated) and one unit of time is an attempted move of every spin.

In infinitely rapid quenches from infinite temperature we took a fully random initial condition in which a random number θ_i in the interval $[-\pi, \pi]$ is associated to site i . We explain the implementation of more sophisticated cooling procedures in Sect. 5.

The focus of our study is the evolution of the number of vortices. We determine it numerically with two types of measurements. On the one hand dynamic scaling implies that the density of vortices, ρ_v , should depend on the typical growing length, ξ , as $\rho_v \simeq \xi^{-2}$. We shall use several determinations of ξ that include the exponential decay of the two-point correlation function, $C[\xi_c(t, T), t] = \text{const.}$, and the second moment of $C(r, t)$, that is defined as follows [31]. From the total magnetization $\vec{M}(t) = \sum_i \vec{s}_i(t)$ and the magnetic susceptibility

$$\chi(t) = \frac{1}{L^2} \vec{M}^2(t), \quad (3)$$

the second moment correlation length on a lattice of size L^2 is defined by

$$\xi_2^2(t) = \frac{1}{(2\sin(\pi/L))^2} \left(\frac{\chi(t)}{F(t)} - 1 \right), \quad (4)$$

where

$$F(t) = \frac{1}{L^2} \sum_{ij} \langle \vec{s}_i(t) \cdot \vec{s}_j(t) \rangle \cos(2\pi(j_x - i_x)). \quad (5)$$

In addition, we determine the number of vortices N_v directly from the configuration of the system by counting the plaquettes with non-zero vorticity. The vorticity is determined as the integer winding number n , so that the phase difference $\theta_{ij} \equiv \theta_i - \theta_j$ around the plaquette is equal to $\sum \theta_{ij} = 2\pi n$. The number of vortices N_v is then obtained as the number of plaquettes around which the phase θ_i rotates through $\pm 2\pi$, taking care that the phase difference θ_{ij} is restricted to the interval $[-\pi, \pi]$, as are the phases θ_i . The density of vortices is then $\rho_v = N_v/L^2$.

In the figures we will not report the statistical errors because they are very small for the quantities we consider (smaller than dot dimensions in the various plots). For example, for the largest system size ($L = 400$) for which the fluctuations are larger, the variance of the number of vortices is at most 3 to 4%.

2.2.2 Time-dependent Ginzburg-Landau equation

A field theory version of this problem, better suited for analytic calculations is given by the time-dependent Ginzburg-Landau equation that determines the stochastic evolution of the coarse-grained two-component field $\vec{\phi}$:

$$\frac{\partial \vec{\phi}(\vec{r}, t)}{\partial t} = -\Gamma \frac{\delta H}{\delta \vec{\phi}(\vec{r}, t)} \quad (6)$$

with Γ the kinetic coefficient. The ‘free-energy’ is

$$H = \int d^2r \left[\frac{\rho_s}{2} (\vec{\nabla} \vec{\phi}(\vec{r}))^2 + \frac{u}{4} (\phi^2(\vec{r}) - 1)^2 \right] \quad (7)$$

with ρ_s the stiffness coefficient or elastic constant and $u > 0$ the strength of the non-linearity that drives the vector field to take unit modulus. Noise can be added to Eq. (6) in the form of an additional stochastic term in its right-hand-side with Gaussian statistics and, typically, delta-correlated, $\langle \zeta_a(\vec{r}, t) \zeta_b(\vec{r}', t') \rangle = 2k_B T \Gamma \delta_{ab} \delta(\vec{r} - \vec{r}') \delta(t - t')$, with $a, b = 1, 2$. The analytic predictions on the time-dependent growing length to be discussed in Sect. 4.1 have been obtained using this approach [32, 33].

3 The BKT equilibrium phase transition

We summarize the static properties of the $2d$ XY model as figured out by Berezinskii [28] and Kosterlitz and Thouless [29] (the BKT picture).

In the thermodynamic limit $2d$ XY models display no conventional long-range order (the magnetization vanishes at all temperatures due to spin-wave excitations) but topological order below a critical temperature T_{KT} . The physics is dominated by two types of excitations: harmonic spin waves and vortices. The former are responsible for destroying conventional long-range order while the latter are responsible for the phase transition. The Berezinskii-Kosterlitz-Thouless (BKT) phase transition at T_{KT} is characterized by a change in the behaviour of the equilibrium spatial correlation function $C(r) = \langle \vec{s}_i \vec{s}_j \rangle_{|\vec{r}_i - \vec{r}_j| = r}$ where the angular brackets denote an average over the equilibrium measure. The high- T phase is disordered, the correlation decays exponentially,

$$C(r) \simeq e^{-r/\xi_{eq}}, \quad (8)$$

and there is a finite density of free vortices. Close and above T_{KT} the correlation length diverges exponentially

$$\xi_{eq} \simeq a_\xi e^{b_\xi [(T - T_{KT})/T_{KT}]^{-\nu}} \quad (9)$$

with $\nu = 1/2$ and b_ξ a non-universal constant that typically takes a value of order one (on a square lattice $b_\xi \sim 1.5$) [28, 29]. Thermodynamic quantities are smooth across the transition. The low- T phase has quasi-long-range order,

$$C(r) \simeq r^{-d+2-\eta(T)} = r^{-\eta(T)}, \quad (10)$$

it is critical in the sense that the equilibrium correlation length diverges, $\xi_{eq} \rightarrow \infty$, and it is characterized by the T -dependent exponent $\eta(T)$ [29] that decreases upon decreasing temperature from $\eta(T_{KT}) = 1/4$ to $\eta(T \rightarrow 0) = T/(2\pi J)$. Bound vortex-antivortex pairs populate the low-temperature ordered phase coexisting with spin-waves. The transition is interpreted by using an analogy with the Coulomb gas in which the system has a low-temperature dielectric phase (with charges, in the $2d$ XY case vortices, bound into dipoles) and a high-temperature plasma or conducting phase with free charges (in the $2d$ XY model vortices) [28, 29]. In short, at T_{KT} pairs dissociate.

The BKT singularity yields the best fit to data generated with large-scale Monte Carlo simulations and short-time dynamics. The data tend to confirm the analytical values of the exponents ν and $\eta(T)$ and the critical temperature was estimated to $T_{KT} \simeq 0.89$ [34, 35, 36, 37, 38]. In finite size systems the effective transition temperature behaves as $T_{KT} + O(\ln^{-2} L)$ [39]. Monte Carlo values of the correlation length $\xi_{eq}(T)$ obtained with lattices with linear size $L = 512$ are $\xi_{eq}(1.25) \simeq 3.8$, $\xi_{eq}(1.04) \simeq 18.7$, and $\xi_{eq}(0.98) \simeq 70$ [35]. We shall discuss our own data, obtained with much smaller system sizes, in Fig. 11.

4 Relaxation after a quench

The nonequilibrium behavior of the $2d$ XY model following an instantaneous quench below T_{KT} has been studied theoretically as well as experimentally [7,

40]. In this Section we recall the time-dependence of the growing correlation-length. We go beyond this by-now well-established aspect of the dynamics with a careful analysis of the temperature-dependence that will be of use in the rest of the article. We present a detailed analysis of the vortex-anti-vortex time-dependent structure.

4.1 Analytic prediction for the growing length

In this Section we set the origin of time to be the instant at which the initial condition is let evolve in the new parameter conditions. At all $T \leq T_{KT}$ a system prepared in an out of equilibrium initial state approaches equilibrium through a coarsening process in which local – critical – equilibrium is established over a length scale $\xi(t, T)$. The space-time correlation $C(r, t) = \langle \vec{s}_i(t) \vec{s}_j(t) \rangle_{|\vec{r}_i - \vec{r}_j| = r}$ is governed by the scaling form

$$C(r, t) \simeq r^{-\eta(T)} f\left(\frac{r}{\xi(t, T)}\right). \quad (11)$$

$\eta(T)$ is the static critical exponent. The scaling function depends on the initial conditions. We focus on high-temperature, disordered ones. $f(0) = 1$ so that the equilibrium result (10) is recovered for all $a \ll r \ll \xi(t, T)$, a being a microscopic cut-off length, and, in particular, in the infinite long time limit in which $\xi(t, T) \rightarrow \infty$. In the opposite limit $r \gg \xi(t, T)$ the system remains disordered, as in the initial condition, and this is ensured by an $f(x)$ that rapidly falls-off for $x \gg 1$.

The relaxation of an out of equilibrium state is due to two processes: the dynamics of Goldstone modes and the annihilation and pairing of vortices. One can tune the importance of the vortex contribution by choosing the initial condition. For example, a completely ordered configuration is free of vortices while a high temperature configuration has a finite density of free vortices. After taking a fully ordered initial condition to $0 < T < T_{KT}$, no free vortices are generated by thermal fluctuations and the system orders in the new conditions by growing a length $\xi(t, T) \propto [\lambda_0(T)t]^{1/2}$ [41, 42]. Instead, the relaxation of an initial condition with free vortices in the critical low-temperature phase is far more interesting. Whether dynamic scaling holds and, in the affirmative, which is the time-dependent growth-law was a subject of debate for some time. The following scenario is well-established now.

The numerical integration of the zero-temperature Ginzburg-Landau equation using fully random initial conditions (with, on average, a density of vortices of $1/3$) first suggested a power-law for $\xi(t, T)$ with a small but measurable deviation from the diffusive law $t^{1/2}$ [43, 44]. This regime was considered to be a transient fully determined by the vortex annihilation dynamics. Yurke *et al.* [32] and Bray *et al.* [33] built upon these results and gave an argument for

$$\xi(t, T) \simeq \left\{ \lambda(T) \frac{t}{\ln[t/t_0(T)]} \right\}^{1/z} \quad z = 2 \quad (12)$$

in quenches from equilibrium at $T \geq T_{KT}$ to $T = 0$, see below. For the sake of completeness, we wrote this expression inserting the dynamic exponents z ($= 2$ in this case). The extension to finite working T was worked out in [45]. This law was confirmed by extensive zero-temperature numerical simulations in [46, 47]. The parameter $\lambda(T)$ and the microscopic cut-off $t_0(T)$ are non-universal in the sense that they depend on the procedure used to measure ξ .

Let us briefly reproduce here the argument that leads to (12) and extend it later to infer the relaxation time. Within the Ginzburg-Landau model (6), a field configuration, describing a single free vortex $\vec{\phi} = \vec{r}/r$ has an energy $E_v = \pi\rho_s \ln(L/a)$, where L and a are the system size and microscopic cut-off (*e.g.*, the lattice spacing). In the many-vortex situation, where $\xi(t)$ represents the typical spacing between vortices and anti-vortices one can derive the following expression for the typical speed of a vortex [32, 45]

$$\frac{d\xi(t)}{dt} \simeq \frac{\rho_s \Gamma}{\xi(t) \ln[\xi(t)/a]} \quad (13)$$

from the zero temperature time-dependent Ginzburg-Landau equation (6). The solution is Eq. (12) with $t_0 \simeq a^2/\rho_s \Gamma$. We assume, following [45], that this equation holds at finite T , and even above T_{KT} where, though, the growing length saturates to the equilibrium correlation length at sufficiently long times. Matching the growing length with the equilibrium law by $d\xi/dt|_{\xi_{eq}} \simeq \xi_{eq}/\tau_{eq}$ above T_{KT} one finds

$$\tau_{eq} \simeq \xi_{eq}^z \ln(\xi_{eq}/a). \quad (14)$$

An exponential divergence of τ_{eq} with the distance to criticality is recovered by substituting ξ_{eq} with the expression in (9):

$$\tau_{eq} \simeq a_\tau e^{b_\xi z[(T-T_{KT})/T_{KT}]^{-\nu}} \left(\frac{T-T_{KT}}{T_{KT}} \right)^{-\nu}. \quad (15)$$

The same behavior is estimated in [48] with a different argument.

4.2 Numerical measurements of the growing length

Although different determinations of the growing length should converge, asymptotically to the same and unique law, some are more convenient than others at finite times. Comparison of different prescriptions (from scaling of the space-time correlation, the density of topological defects, and the structure factor) were discussed in [46, 47]. We revisit this issue with the purpose of clarifying the different rôle played by bound and free vortices and establishing the temperature dependence of the correlation length.

In Fig. 1 we extract the growing length $\xi(t, T)$ from the decay of the space-time correlation. In the left panel we show the bare data, and we confirm that C satisfies dynamic scaling by using the value of $\xi_c(t, T)$ inferred from the condition $C[\xi_c(t, T), t] = 0.3$. In the right panel we compare the time-dependence of $\xi_c(t, T)$ to the power law $t^{1/2}$ and we see the expected slower

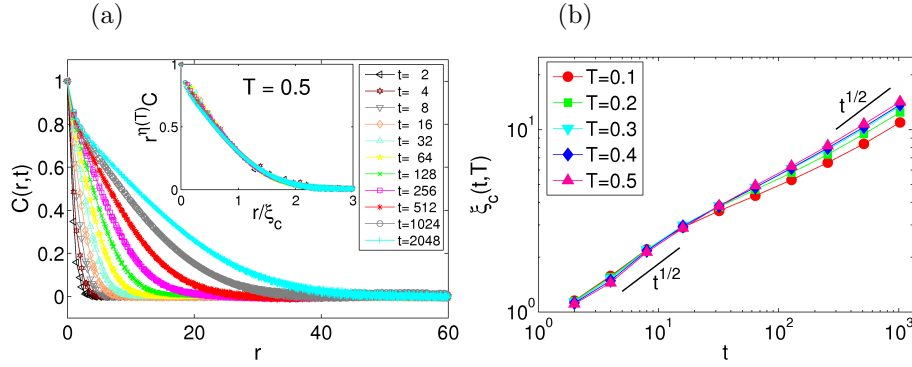


Figure 1: (Color online.) Space-time correlation after an infinitely rapid quench from a fully random initial condition into the low temperature phase. (a) Bare data for $C(r,t)$ at different times t after a quench to $T = 0.5$ that are given in the key. The inset shows the scaling plot $r^{\eta(T)} C$ against $r/\xi_c(t,T)$ using $\xi_c(t,T)$ computed from $C[\xi_c(t,T), t] = 0.3$. (b) $\xi_c(t,T)$ against t for instantaneous quenches to different temperatures.

growth at sufficiently long times. The small deviations due to the logarithmic correction will be studied in more detail in Fig. 2.

Next we analyze the growing length as extracted from the density of vortices. In the fully random, infinite temperature limit, $\rho_v \simeq 0.3$. In equilibrium at $2T_{KT}$ we found a value slightly smaller than 0.2 in agreement with data shown in [35]. After the infinitely rapid quench the very high density of free vortices present in the initial high temperature condition decreases. Two processes contribute to the re-organization of the vortex configuration. On the one hand over-abundant defects annihilate. On the other hand vortices and anti-vortices bind to approach the non-vanishing equilibrium density of pairs, $\rho_{eq} \simeq e^{-2\mu/T}$ with $\mu \simeq 3.77$ [35], that is an increasing function of T .

According to dynamic scaling, during the out of equilibrium relaxation the density of defects in the ordered phase should decrease as $\rho_v(t,T) \simeq 1/\xi_v^2(t,T)$ that using eq. (12) is equivalent to $\rho_v(t,T) \ln \rho_v(t,T) \simeq t^{-1}$ [32]. In Fig. 2 we show our data for all vortices in two ways: in the left panel we plot $\rho_v(t)$ as a function of t for several values of T ; in the right panel $N_v(t) \ln N_v(t)$ as a function of t where N_v is the number of vortices selecting the case $T = 0.4$. After one MC step the density is very close to the initial value $\rho_v(T \rightarrow \infty) \simeq 0.3$ but it subsequently monotonically decreases in time in all cases. As already stressed by Yurke *et al.* [32], who solved numerically the time-dependent Ginzburg-Landau equation with noise, the second presentation gives a much better description of data for $T \lesssim 0.4$, confirming the growth-law (12). However, at T close to T_{KT} the number of vortices gets close to the equilibrium value, for example $\rho_{eq} \simeq 10^{-4}$ at $T = 0.8$, and the cross-over to equilibrium dynamics is reached within the simulation times. This is accompanied by the generation of many

short-lived vortex anti-vortex pairs, similar to what was observed in [32], and the data deviates from the expected scaling. The failure of scaling of the space-time correlation when ξ_v is used was also mentioned in [46, 47].

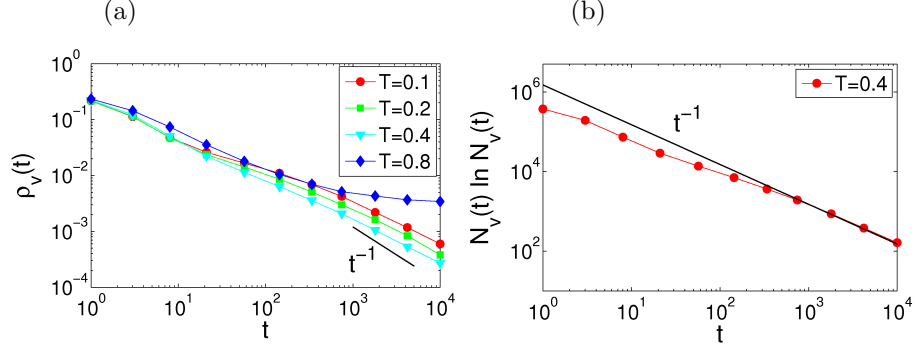


Figure 2: (Color online.) Time-dependence of the total density of vortices, $\rho_v(t, T) \equiv N_v(t, T)/L^2$, after an infinitely rapid quench from $T_0 \rightarrow \infty$ to $0 \leq T \leq T_{KT}$ given in the key. The data are shown in the form $\rho_v(t)$ vs. t in (a) and $N_v \ln N_v$ vs. t at a relatively low T in (b). The former display the deviation from the ‘diffusive’ t^{-1} law. The latter confirms the expected logarithmic correction to a power law decay. The T -dependence and, especially, the saturation observed at high T are discussed in the text.

A more precise determination of the growing length at temperatures close to T_{KT} should be given by the evolution of the density of free vortices only, ρ_v^f . The identification of free vortices involves, however, some ambiguity. We used a simple-minded form that consists in counting as free all vortices and antivortices that do not have a neighbour of opposite vorticity at Euclidean distance $r \leq r_c$. By varying the parameter r_c from 1 to 2 we found that the second choice gives very good results, shown in Fig. 3 in the form $N_v^f \ln N_v^f$ against t for $T = 0.4, 0.6, 0.8$. (In [51] r_c is chosen to be equal to $\xi(t, T)$.) Consistently, $\xi_v^f \simeq \xi_v$ at sufficiently low temperatures (say, $T \leq 0.4$) but the two depart at higher temperatures, with the former yielding the correct out of equilibrium correlation length and being the one that ensures dynamic scaling.

4.2.1 Temperature dependence

The T -dependence in λ and t_0 in Eq. (12) has not been fully established yet. The assumption that at finite temperature the dynamics on scales that are shorter than $\xi(t, T)$ should be described, in the limit of large $\xi(t, T)$, by renormalized spin-wave theory [33, 45] suggests $\lambda(T) = \rho_s(T)\Gamma(T)$ and $t_0(T) = a^2/[\rho_s(T)\Gamma(T)]$ at all $T \leq T_{KT}$. a is the lattice spacing or microscopic cut-off, ρ_s the renormalized spin-wave stiffness and Γ the renormalized kinetic coefficient in the time-dependent Ginzburg-Landau model. The numerical data in [37]

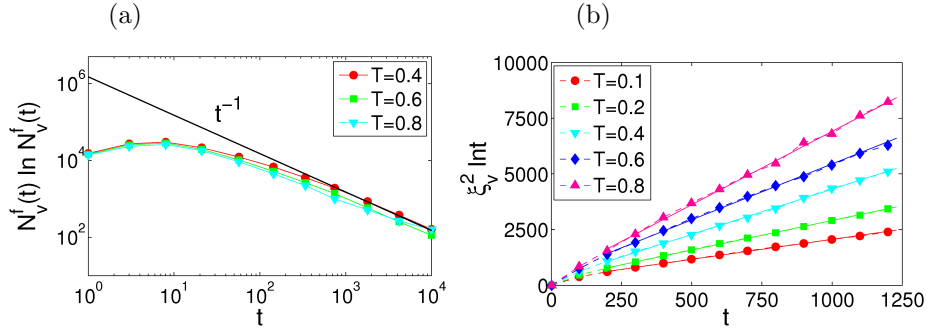


Figure 3: (Color online.) (a) Time-dependence of the density of free vortices, expressed in the form $N_v^f(t) \ln N_v^f(t, T)$ against t , after an infinitely rapid quench from $T_0 \rightarrow \infty$ to $0 \leq T \leq T_{KT}$ given in the key. (b) Time-dependence of the growing correlation length, defined as $\xi_v \equiv (\rho_v^f)^{-1/2}$ for values of T given in the key. Vortices and antivortices are considered to be free when the distance to their closest neighbour of the opposite vorticity is larger than a cut-off that in this figure has been chosen to be $r_c = 2$ lattice spacings.

analyzed with an effective power-law $\xi(t, T) \simeq \bar{\lambda}(T)t^{1/z(T)}$ yield an effective T -dependent exponent that slowly increases with decreasing T . This is consistent with a microscopic time-scale $t_0(T)$ in Eq. (12) that also weakly increases upon decreasing temperature. This in turn implies that $\lambda(T)$ is a weakly increasing function of T . We analyzed the T -dependence of the parameters λ and t_0 by plotting

$$\xi^2(t, T) \ln t \quad \text{against} \quad t \quad (16)$$

in Fig. 3 (b) and 4 (a), using ξ_v^f and ξ_2 , respectively. Since the microscopic time t_0 cannot be determined precisely due to the relatively long transient needed to reach the asymptotic law, and the fact that it yields a sub-dominant contribution anyhow, we fix it to one and determine the remaining free-parameter λ . The data fall on straight lines with slope $\lambda(T)$. For all temperatures simulated, $\lambda(T)$ is an increasing function of temperature. As the temperature approaches T_{KT} , $\lambda(T)$ as obtained from the density of all vortices decreases, see Fig. 4. As already explained, this is an artifact of not having distinguished free from bound vortices. The agreement between the trend obtained from ξ_2 and ξ_v^f is very satisfactory. The dashed line is a linear fit to the datapoints, $\lambda(T) \simeq \lambda_0 + cT$ with $\lambda_0 \simeq 1.2$ and $c = 6.8$.

The T -dependence of t_0 and λ are consistent with Berthier *et al*'s recognition that the Monte Carlo generated vortex configurations at a given waiting-time after a quench to different temperatures are rather different. At high T (although below T_{KT}) the vortices tend to form pairs, as they should in equilibrium below T_{KT} , while at lower T there are more free vortices. The suggestion is that the dynamics are faster at higher T (since vortex diffusion is faster) than at lower T [42].

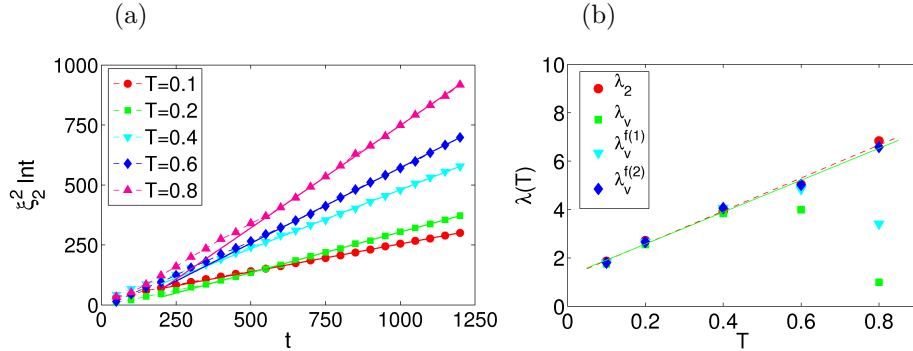


Figure 4: (Color online.) Temperature dependence of the parameter $\lambda(T)$ in the growth law (12) after an instantaneous quench from infinite temperature into the ordered phase. (a) The growing length determined as $\xi_2(t, T)$. The slope in the long-time limit is $\lambda(T)$ and it increases with increasing T for all T 's studied. The time-scale $t_0(T)$ cannot be determined due to the long transient. (b) $\lambda(T)$ using four determinations: ξ_2 , the total density of vortices and the density of free vortices with $r_c = 1$ and $r_c = 2$. The agreement between the first and the last one is very good.

4.3 Spatial structure

Further information on the vortex anti-vortex pair structure is obtained from the analysis of pair correlation functions that ignore or take into account the polarity of the vortices. In the former case we define a variable n_i that equals 1 if the site i is occupied by a defect irrespective of its polarity and 0 otherwise. In the latter the variable n_i takes three values; $n_i = 1$ if the site is occupied by a vortex, $n_i = -1$ if it is occupied by an anti-vortex, and $n_i = 0$ if there is no defect. The correlation function is then defined as $G(r, t) = \langle n_i(t) n_j(t) \rangle$ where $r = |\vec{r}_i - \vec{r}_j|$ in both cases. The first type of correlation does not yield additional information on the behaviour of the system with respect to $C(r, t)$ studied above. Instead, the latter has a minimum at the preferred distance between vortices and anti-vortices [50]. In Fig. 5 we study $G(r, t)$ at several instants after the quench, showing in (a) the raw data in the form $rG(r, t)$ against r and in (b) the scaling plot $\xi_v^3(t, T)rG(r, t)$ against $r/\xi_v(t, T)$ with $\xi_v(t, T)$ the correlation length obtained from the analysis of the density of free vortices (similar results are obtained using ξ_2). The data confirm that this quantity is well described by dynamic scaling. The scaling function has a minimum at $r \simeq 0.48 \xi_v$ and it oscillates with very small amplitude around zero at long distances, a feature observed experimentally [49] but not captured by the approximate theory in [50].

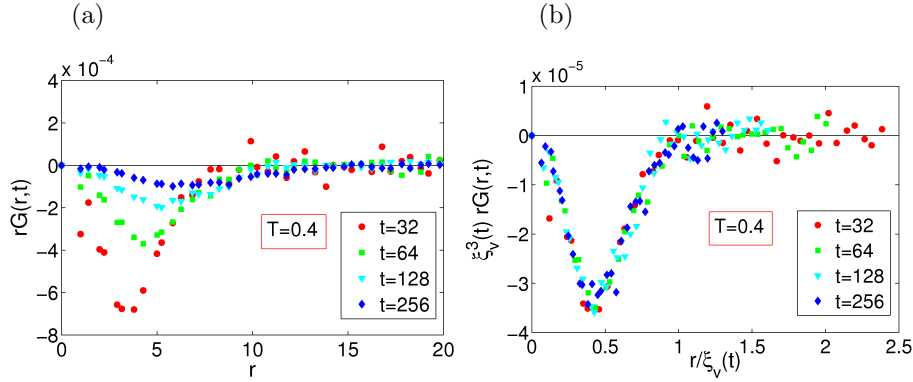


Figure 5: (Color online.) Polarity correlation function. (a) $rG(r, t)$ against r at different times t after the quench into the low-temperature phase. (b) Scaling plot $\xi_v^3(t)rG(r, t)$ against $r/\xi_v(t)$ with $\xi_v(t)$ the length extracted from the analysis of the density of free vortices. The numerical data have been smoothened.

4.4 Pair distribution function

MC simulations give us access to the distances between vortices and anti-vortices and, in principle, to their pairing. The assignment of pairing is, however, a hard problem not free from ambiguity. We used the following simple algorithm. Given a configuration, we first computed and ordered all distances between vortices and anti-vortices. However, the lattice structure implies that, for sufficiently high density, some vortex (or anti-vortex) could be at equal distance from two (or more) anti-vortices (or vortices). In these cases we chose the pairing at random and we continued the procedure with the remaining defects. With this method we are not sure of finding the optimal pairing but, statistically, we expect all these pairings to be equivalent as the distribution of distances is concerned, a feature that we verified numerically. An example of the pair-distance construction is shown in Fig. 6. In panel (a) the configuration at $t = 100$ MCs after a quench from $T_0 \rightarrow \infty$ to $T = 0.4$ is represented as a Schlieren pattern in which a gray scale is proportional to $\sin^2(2\phi)$ with ϕ the angle formed by the local spin and the x axis. Each vortex emanates eight brushes of alternate black and white color. In panel (b) the vortices and anti-vortices are shown with (red) pluses and (blue) squares. A few pairings, as obtained with our simple algorithm, are highlighted in grey.

Figure 7 displays the evolution of the distribution of pair distances after a quench from infinite temperature to $T = 0.4$. The log-log plot in panel (a) demonstrates that the initial probability distribution function (pdf) is a power law, $\simeq r^{-\tau}$ with $\tau \simeq 3.5$. Similarly to what was found in the study of geometric properties of coarsening in the Ising universality class [52], small linear scales – as compared to ξ_v – change significantly in time while larger scales do not.

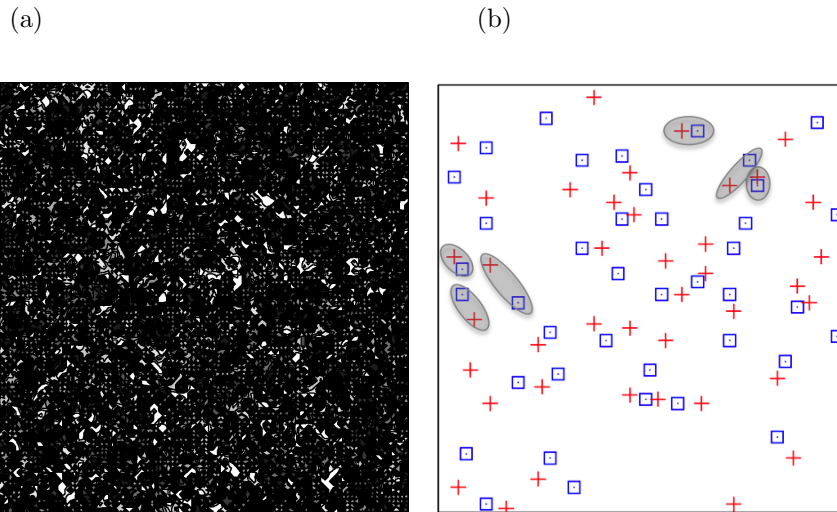


Figure 6: (Color online.) Defect configuration at $t = 100$ MCs after quenching the sample to $T = 0.4$ in the ordered phase. The configurations are shown as Schlieren patterns over the full lattice ($L = 100$) on the left panel. The gray scale is proportional to $\sin^2(2\phi)$ with ϕ the angle formed by the local spin and the x axis. On the right panel, the vortex configurations at time $t = 100$ are shown. Vortices are represented by (red) pluses and antivortices by (blue) squares. The total number of vortices in the system is $N_v(t = 100) = 80$. We graphically show a few pairing of vortices and antivortices.

This means that the tail of the distribution remains the initial power-law for $r \gg \xi_v(t)$ while the weight on smaller scales decreases significantly as a function of time. Panel (b) presents the scaling plot, $\xi_v^4 N_p(r, t)$ against $r/\xi_v(t)$, in which one confirms that dynamic scaling is well satisfied. The crossover at $r \simeq \xi_v(t)$ is clear in the figure. The kind of oscillating features at very short distances, $r \lesssim 3$, might be due to the discrete lattice.

The data in Fig. 7 is to be compared to results shown in Fig. 1 of Ref. [30]. The latter were obtained using the Fokker-Planck equation for the density of pairs of separation between r and $r + dr$ proposed in [53]. This equation is tailored to hold at $T \leq T_{KT}$, it does not take into account the effect of free vortices, and it does not capture the logarithmic correction to the diffusive growing length. The quench is done from equilibrium at T_{KT} , where the distribution is the power law $r^{-\tau}$ with $\tau \simeq 4.70$, to a very low T . The qualitative features of the two sets of data are the same. However, the quantitative properties are not. The initial conditions, and hence the initial distributions, are different. The time-dependent part has a peak in our case and it is totally flat in [30]. Our pdf satisfies scaling with respect to the correct growing length.

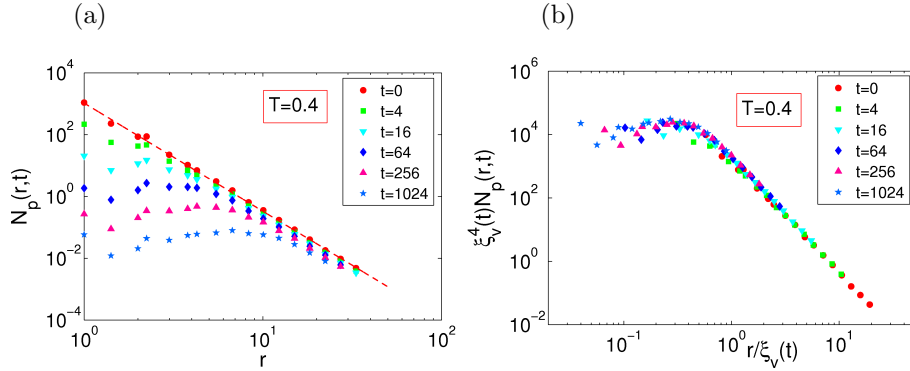


Figure 7: (Color online.) Number of vortex-antivortex pairs, N_p , as defined in the text, after the quench from $T \rightarrow \infty$ to $T = 0.4$. (a) N_p as a function of their distance r at different times given in the key. The dashed line is a guide-to-the-eye representing the power $r^{-3.5}$. (b) Scaling plot.

5 Dynamics after a slow cooling

In this Section we discuss the evolution of the system after a slow cooling from high T to its low T phase. The cooling procedure used is graphically represented in Fig. 8 and it consists in the following. We suddenly quench the sample from $T \rightarrow \infty$ (random initial condition) to T_0 . In practice, we chose $T_0 = 2T_{KT}$. We let the system evolve at this temperature a large number of MCs, typically $t_{rel} = 2 \times 10^5$ to 6×10^5 depending on the system size. Equilibration occurs relatively rapidly far from T_{KT} so for all purposes we can assume the system to be in equilibrium at $2T_{KT}$. We then cooled the sample by changing the temperature linearly in time according to

$$T(t) = T_{KT}(1 - t/\tau_Q) \quad -\tau_Q \leq t \leq \tau_Q. \quad (17)$$

Within this time reference, annealing from $2T_{KT}$ starts at $t = -\tau_Q$. At negative times t the system is above the phase transition, at $t = 0$ it reaches T_{KT} and at positive times it enters the ordered phase. τ_Q is the inverse cooling rate. At $t = \tau_Q$ the environmental temperature vanishes and times are naturally bounded by τ_Q . See Fig. 8 for a graphical representation of these cooling rate procedures. Although more complicated cooling procedures are also of interest, and have been analyzed in detail in the 1d Glauber Ising chain [13], we shall not discuss them here.

5.1 Snapshots

A first intuitive understanding of the defect density left over in the ordered phase after a slow annealing through the phase transition is obtained by looking at the spin configurations.

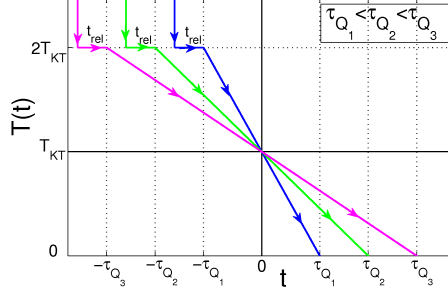


Figure 8: (Color online.) Sketch of the cooling procedures used.

In Fig. 9 we display the system configuration on a section of linear size $L = 100$ of a system with size $L = 256$ at $t = 200$ MCs after having crossed the phase transition with two inverse cooling rates $\tau_Q = 256, 2048$ MCs. Note that the temperature at which the snapshots are taken is different, $T(t = 200, \tau_Q = 256) = 0.2$ [(a) and (b)] and $T(t = 200, \tau_Q = 2048) = 0.8$ [(c) and (d)]. The figure demonstrates that the density of vortices increases with increasing τ_Q , with $N_v = 186$ in the first case and $N_v = 352$ in the second.

In Fig. 10 we show four configurations at $t = \tau_Q$, when the temperature has reached the value zero, with $\tau_Q = 128, 512, 1024, 2048$ MCs from (a) to (d), respectively. It is clear from the figure that the density of vortices decreases with increasing τ_Q . We measured $N_v = 180, 92, 68, 42$ for increasing τ_Q . In the following we shall make these statements quantitative.

5.2 Equilibrium – out of equilibrium crossover

The annealing procedure occurs by the following steps. In the high temperature phase the system is plagued with free vortices and anti-vortices. The initial state thus contains a large number of free defects. Let us assume that the system is in equilibrium at T_0 ($= 2T_{KT}$ in our simulation). Under the cooling procedure, if this is slow enough, it evolves adiabatically, *i.e.*, it remains instantaneously in equilibrium at $T(t)$. The equilibrium correlation length is swept in time according to

$$\xi_{eq}(t) \simeq a_\xi e^{b_\xi |t/\tau_Q|^{-\nu}} \quad (18)$$

and the density of vortices, estimated from $\rho_v(t) \simeq \xi_{eq}^{-2}(t)$, decreases exponentially:

$$\rho_v(t) \simeq a_\xi^{-2} e^{-2b_\xi |t/\tau_Q|^{-\nu}}. \quad (19)$$

However, this regime cannot last for ever, it crosses over to a different, much slower one, when the system falls out of equilibrium due to the fact that the relaxation time becomes much longer than the parameter variation imposed by the cooling rate procedure. Indeed, using τ_{eq} as derived in (15) and replacing

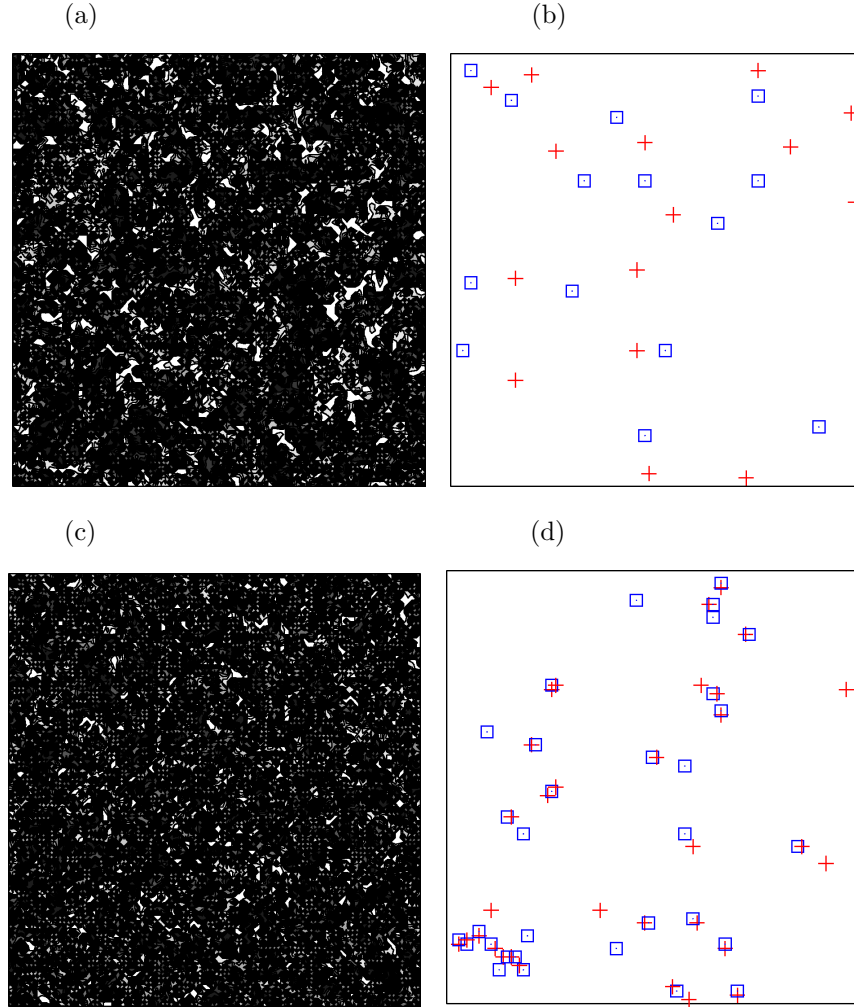


Figure 9: (Color online.) Comparison between the defect configuration at $t = 200\text{MCs} < \min(\tau_Q)$ after annealing the sample into the ordered phase with two different inverse cooling rates $\tau_Q = 256$ MCs and 2048 MCs. We show parts of linear size 100 of the full lattice $L = 256$. The configurations are shown as Schlieren patterns on the left [(a) and (c)]. The gray scale is proportional to $\sin^2(2\phi)$ with ϕ the angle formed by the local spin and the x axis. On the right side, the vortex configurations at time $t = 200$ are shown [(b) and (d)]. Vortices are represented as (red) pluses and antivortices by (blue) squares. The total numbers of vortices in the system are $N_v = 186$ for the fast cooling in which $T = 0.2$ is reached and $N_v = 352$ for the slow one in which the configuration is measured at $T = 0.8$.

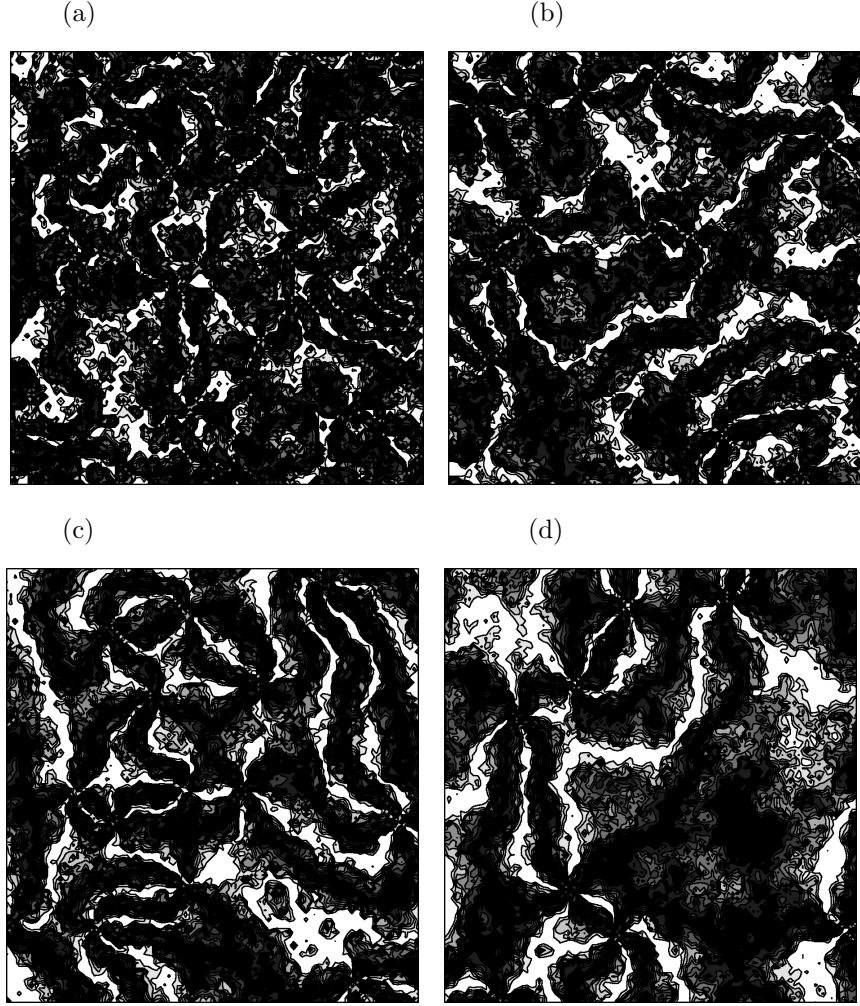


Figure 10: (Color online.) Comparison between the defect configuration at $t = \tau_Q$ after annealing the sample to $T = 0$ with four different inverse cooling rates $\tau_Q = 256$ (a), 512 (b), 1024 (c) and 2048 (d). We show a section of linear size 100 of the full lattice with $L = 256$. The total number of defects decreases with increasing τ_Q and are $N_v = 180, 92, 68, 42$ from (a) to (d).

$T(t)$ by its time-dependence, one finds

$$\tau_{eq}(t) \simeq a_\tau e^{zb_\xi |t/\tau_Q|^{-\nu}} |t/\tau_Q|^{-\nu}. \quad (20)$$

The system can no longer follow the pace of evolution set by the changing conditions. The crossover is estimated as the moment when the relaxation time τ_{eq} reaches the characteristic time of variation of the temperature¹ $\Delta T/d_t \Delta T = -\hat{t}$ [15]. The crossover occurs above the critical temperature, $\Delta T \equiv T - T_{KT} > 0$ and $\hat{t} > 0$. The negative time $-\hat{t}$ is computed by assuming that the crossover occurs close to the transition, so that the critical scaling (9) determines the equilibrium relaxation time τ_{eq} . One then has $|\hat{t}| \simeq \tau_{eq}(-\hat{t})$ and

$$\hat{t} \simeq a_\tau (\hat{t}/\tau_Q)^{-\nu} e^{zb_\xi (\hat{t}/\tau_Q)^{-\nu}}. \quad (21)$$

The τ_Q dependence of \hat{t} can be obtained numerically through the Lambert W function, *i.e.*, the inverse of $f(x) = xe^x$. An analytic argument to get the leading τ_Q dependence relies on recasting (21) as

$$(1 + \nu) \ln x + \ln(\tau_Q/a_\tau) \simeq b_\xi z x^{-\nu} \quad \text{with} \quad x \equiv \hat{t}/\tau_Q. \quad (22)$$

Assuming that the solution is such that $x \rightarrow 0$ with $\tau_Q/a_\tau \rightarrow \infty$ we find, in first approximation,

$$x \equiv \frac{\hat{t}}{\tau_Q} = \frac{\hat{T} - T_{KT}}{T_{KT}} \simeq \left(\frac{b_\xi z}{\ln(\tau_Q/a_\tau)} \right)^{1/\nu}, \quad (23)$$

that is consistent with the assumption. \hat{t} is smaller than τ_Q – due to the logarithmic correction – and this is in agreement with the fact that the system should fall out of equilibrium after the beginning of the annealing procedure at $t = -\tau_Q$. Plugging now the ‘first order’ solution (23) in Eq. (22), we find a further logarithmic correction:

$$x \equiv \frac{\hat{t}}{\tau_Q} = \frac{\hat{T} - T_{KT}}{T_{KT}} \simeq \left\{ \frac{b_\xi z}{\ln \left[\frac{\tau_Q}{a_\tau} \left(\frac{b_\xi z}{\ln(\tau_Q/a_\tau)} \right)^{(1+\nu)/\nu} \right]} \right\}^{1/\nu}. \quad (24)$$

We compared the numerical solution to Eq. (21) to the estimate (24) for different τ_Q . For small a_τ and $b_\xi \sim 1$ the error is less than 10% for $\tau_Q \gtrsim 200$. Taking into account the full form (24) the correlation length at the crossover reads

$$\hat{\xi} \simeq a_\xi \left\{ \frac{\tau_Q}{a_\tau} \left[\frac{1}{\ln(\tau_Q/a_\tau)} \right]^{(1+\nu)/\nu} \right\}^{1/z}. \quad (25)$$

¹In the 1dIM with Glauber dynamics, a model with an exponential divergence of the relaxation time close to the critical temperature $T_c = 0$, Krapivsky estimates $-\hat{t}$ for generic cooling rates by comparing the time needed to reach the critical point to the relaxation time [13]. For a linear cooling the two definitions are identical.

The length $\xi(t(T), T)$ coincides with the equilibrium correlation length ξ_{eq} for $T(t) > \hat{T}$, when $\xi(\hat{t}, \hat{T})$ reaches $\hat{\xi}$, and $\xi(t(T), T) < \hat{\xi}$ for $T(t) < \hat{T}$. The crossover length, $\hat{\xi}$, increases and the crossover temperature, \hat{T} , decreases with increasing τ_Q . Consequently, one can get closer to the critical point evolving in equilibrium, and thus reach longer equilibrium correlation lengths, for longer τ_Q s.

For the sake of comparison, recall that in a conventional second-order phase transition with power-law divergencies, these quantities are both power laws [15]: $\hat{t}/\tau_Q = (\hat{T} - T_{KT})/T_{KT} \simeq (\tau_Q/a_\tau)^{-1/(1+\nu_{zeq})}$ and $\hat{\xi} \simeq a_\xi(\tau_Q/a_\tau)^{\nu/(1+\nu_{zeq})}$. \hat{t} is also smaller than τ_Q in this case.

5.3 Numerical estimate of the crossover length

In order to put the prediction for $\hat{\xi}$ to the test we compared the equilibrium and growing length extracted from the numerical data. We calculated the equilibrium values using systems with small linear sizes, $L = 16, 20, 30, 50$, that we let equilibrate. In Fig. 11 (a) we display equilibrium data for $\xi_v \propto \rho_v^{-1/2}$ with points. The data for $T \geq 1.2$ do not show finite size effects and are in agreement with the ones in [35] (obtained using much larger samples, $L = 512$) while at lower- T the spread of data is severe and the maximum values found for $L = 50$ are way below the values estimated in [35]. The BKT exponential divergence is reported on the figure with solid line. The dynamic data for $\xi_v[T(t)]$ obtained by using different cooling rates, $\tau_Q = 128, 512, 2048$ MCs, are shown with thin lines in both panels. Finally, the \hat{T} -values at which the dynamic data should diverge from the static ones are signaled with dashed vertical lines. They are obtained from the numerical solution of eq. (21), by using the b_ξ stemming from the fit of the BKT exponential divergence. The parameter a_τ is, on the other hand, determined in such a way that the resulting \hat{T} -values give a good estimate of the divergence of the dynamic data from the static ones.

In Fig. 11 (b) the numerically determined \hat{t} data are compared to the analytic estimate (24). The agreement between Monte Carlo data and analytic estimate is very good within our numerical accuracy.

5.4 Out of equilibrium evolution

At time $-\hat{t}$ close to criticality, the system falls out of equilibrium but it continues to evolve further, from $\hat{T} = T(-\hat{t}) > T_{KT}$ to $T(\tau_Q) = 0$ following the out of equilibrium critical dynamics rules. In the case of a finite rate quench, the total time spent in a critical region includes time \hat{t} , which the system spent above T_{KT} after falling out of equilibrium. That is to say, the total time evolving with critical dynamics is $\Delta t = \hat{t} + t$. Then, we propose to match the equilibrium relaxation above \hat{T} with the critical one below \hat{T} with the asymptotic scaling of

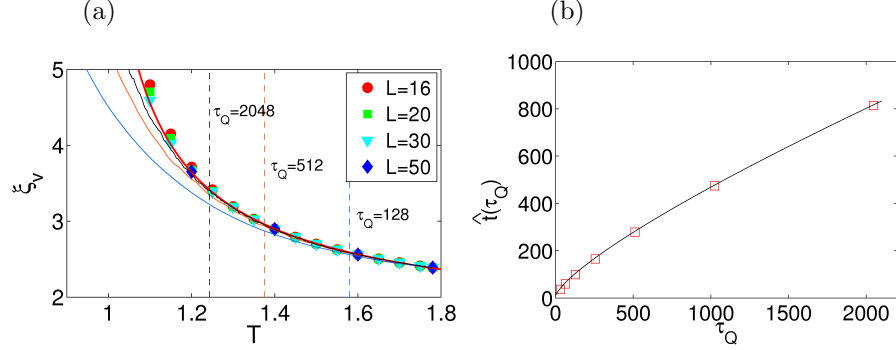


Figure 11: (Color online.) (a) The equilibrium correlation length, ξ_v , at $T > T_{KT}$, for different linear system sizes given in the keys are shown with points. The BKT exponential divergence, as obtained by fitting the data for temperatures higher than $T = 1.2$, where we do not have strong finite size effects, are shown with thick (red) lines. The time-dependent length $\xi_v[T(t)]$ for different cooling rates indicated on the figure are shown with thin lines. The predicted \hat{T} s, for different τ_Q , are signaled with dashed vertical lines. See the text for more details. (b) The crossover time \hat{t} as a function of τ_Q . The data points have been estimated from the numerical simulation – see panel (a) – and the line is the analytic prediction in eq. (24).

the growing length

$$\xi(t) = \begin{cases} \xi_{eq}[T(t)] & t < -\hat{t}(\tau_Q) \\ \hat{\xi} + \left\{ \lambda[T(t)] \frac{\Delta t}{\ln(\Delta t/t_0[T(t)])} \right\}^{1/z} \equiv \xi_{lowT}(t) & t > -\hat{t}(\tau_Q) \end{cases} \quad (26)$$

Note that we assumed that the T -variation of the parameters λ and t_0 should be sufficiently slow so that we can simply replace their time-dependent values in the growth-law after a quench. We shall further fix $t_0 = 1$ as in the quenching case. At $\Delta t = 0$: $T(t) = T(-\hat{t}) = \hat{T}$, $\xi_{eq}(t) = \hat{\xi}$ and these formulæ match.

Let us confront the order of magnitude of the two terms in the second line of eq. (26) for times of the order of the inverse cooling rate, $t \simeq \tau_Q$. Using Eq. (25), the first term is $\hat{\xi} \simeq [\tau_Q / (\ln \tau_Q)^{(1+\nu)/\nu}]^{1/z}$. Since \hat{t} is much smaller than τ_Q , in the long τ_Q limit $\Delta t \simeq \tau_Q$. The λ prefactor is a function of T and hence of t but it should be bounded by the finite and non-vanishing limiting values in Fig. 4. Therefore, apart from the finite prefactor originating in λ , the second term is of the order $\simeq [\tau_Q / \ln \tau_Q]^{1/z}$. Using $\nu = 1/2$, one concludes that the second term, describing the out of equilibrium dynamics below \hat{T} , dominates in the large τ_Q limit. (The same occurs in the conventional second order phase transitions although the mechanism is different [20].) This fact can be observed in panel (a) of Fig. 12 where the growing ξ_v under annealing with seven cooling rates given in the key is shown as a function of the time-varying temperature.

In Fig. 12 we present data for the dynamic growing length for different cooling rates. Panel (a) displays the bare data for seven inverse cooling rates τ_Q given in the key. Panel (b) is scaling plot that tests the hypothesis in Eq. (26) in the low-temperature region during the annealing process. We use the values of the parameter $\lambda[T(t)]$ obtained from the linear fit of data for the quench in Fig. 4. Before rescaling, the correlation length $\xi_v(t)$ grows with time, *i.e.*, with decrease of temperature, in such a way that at a given T , the value of ξ_v increases with τ_Q (see panel (a)). After rescaling with the proposed asymptotic form (26) for $t > -\hat{t}(\tau_Q)$, the values of ξ fall on top of each other. Perfect agreement with the analytic prediction would be the flat master curve $\xi_v(t)/\xi_{\text{low}T}(t) \equiv 1$. The master curve deviates from this prediction but the range of variation is relatively small, varying from 1 to 1.6, *circa*. We ascribe this mismatch to potential non-linear corrections to $\lambda[T(t)]$ and small variations in $t_0[T(t)]$ that we have not taken into account.

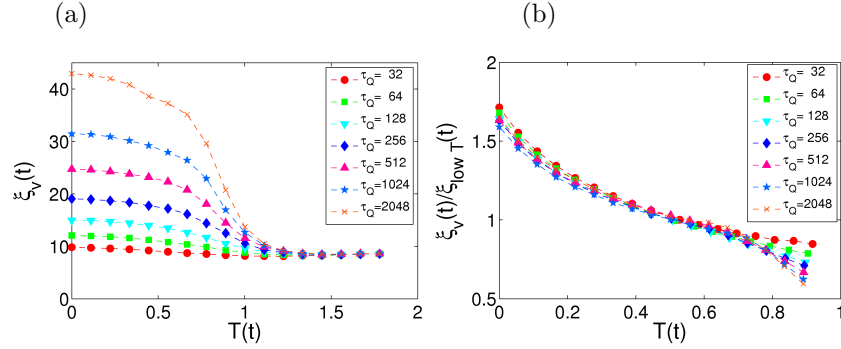


Figure 12: (Color online.) Growing correlation length $\xi_v(t)$ during annealing from $2T_{KT}$ to $T = 0$ with different cooling rates τ_Q . (a) Bare data for seven cooling rates given in the key. (b) Rescaling with the proposed asymptotic form (26) for $t > -\hat{t}(\tau_Q)$.

5.5 Numerical measurements of vortex density

In Fig. 13 we study the density of all vortices during annealing. We present the data obtained by using five cooling rates in a log-log plot. The translation of the x axis by τ_Q is done to give a common origin to all curves as well as to allow for a direct comparison with the results in [30].

Four regimes are evidenced in the figure. At very short times, as compared to a function of τ_Q , the data remain close to the initial and rather large value $\rho_v \simeq 0.2$. This regime crosses over to one with a rapid relaxation in which the density of vortices decreases significantly (the shoulder in the curves). The crossover occurs at $t \gtrsim -\hat{t}$. The relaxation continues in a smoother way and it is close to a power-law decay with logarithmic corrections as expected. This

regime ends when the curves reach the limit of the instantaneously quenched data to $T = 0.4$ that they subsequently follow until $t = \tau_Q$ and $T = 0$. In our setting the density of defects *increases* with increasing τ_Q at fixed $t + \tau_Q$.

The qualitative features of our data are very close to the ones obtained by Chu and Williams [30] for a quench or annealing from equilibrium at T_{KT} to below the critical point. As already said, their method is to solve numerically the Fokker-Planck equation for vortex-pair dynamics in conjunction with the Kosterlitz-Thouless recursion relations derived in [53]. This approach can only be used for initial conditions at and below T_{KT} and does not include the effect of free-vortices. In consequence, the scalings found are consistent with power-laws without logarithmic corrections.

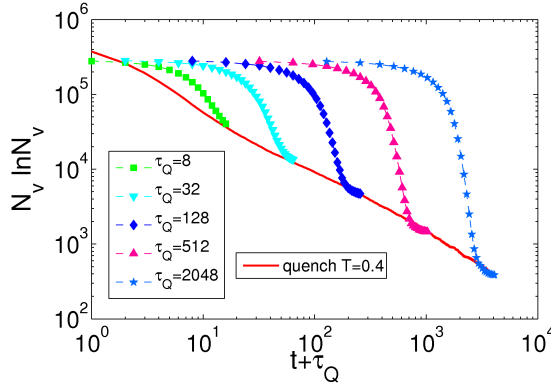


Figure 13: (Color online.) Time-dependence of the total number of vortices after annealing to $T = 0$ with different inverse cooling rates τ_Q given in the key. The data are shown with points in the form $N_v \ln N_v$ as a function of $t + \tau_Q$. With a (red) line we plot the number of vortices after an infinitely rapid quench to $T = 0.4 \leq T_{KT}$.

Finally, we extracted the remanent number of vortices at the end of the cooling procedure, $t = \tau_Q$ and $T = 0$, and we plot it as a function of τ_Q in Fig. 14. The data correspond to the direct counting of (free) defects. The total number of defects varies from 10^4 to 10 circa. On the analytic side, the scaling assumption in Eq. (26) suggest

$$\begin{aligned}
 \rho_v(\tau_Q) &\simeq \tau_Q^{-1} + \left\{ \lambda[T(\tau_Q)] \frac{\Delta t(\tau_Q)}{\ln(\Delta t(\tau_Q)/t_0[T(\tau_Q)])} \right\}^{-1} \\
 &= \tau_Q^{-1} + \left\{ \lambda \frac{(\tau_Q + \hat{t})}{\ln[(\tau_Q + \hat{t})/t_0]} \right\}^{-1} \\
 &\simeq \left\{ \lambda \frac{(\tau_Q + \hat{t})}{\ln[(\tau_Q + \hat{t})/t_0]} \right\}^{-1}
 \end{aligned} \tag{27}$$

where λ and t_0 in the last expression are the zero-temperature values. We

compared the above assumption with the numerical data in Fig. 14 by using the values of \hat{t} obtained numerically in Sect. 5.3 and we found good agreement within our numerical accuracy. The fact that the data points bend at short τ_Q is well captured by the addition of \hat{t} in the numerator. This term becomes negligible for longer τ_Q . At intermediate values of τ_Q the decay can be easily confused with an effective power-law, $\tau_Q^{-0.72}$, shown in the figure with a dashed (blue) line. For longer values of τ_Q the data confirm the logarithmic correction. Note that the decay is slower than in the discrete symmetry breaking case with a low- T phase with trully long-range order, where one finds $\rho_v(t = \tau_Q) \simeq \tau_Q^{-1}$ [20].

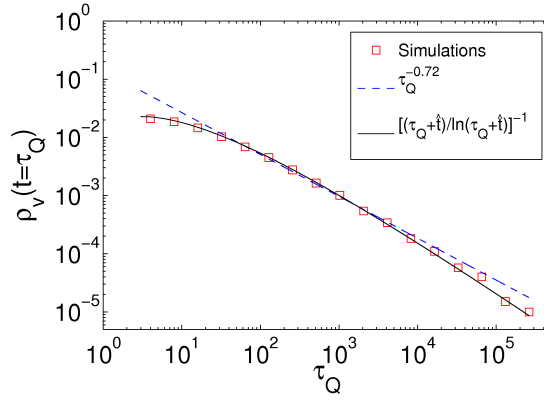


Figure 14: (Color online.) τ_Q -dependence of the density of vortices after annealing the system to $T = 0$. Points represent the numerical data obtained from the direct counting of topological defects, the dashed (blue) line shows an effective power law $\tau_Q^{-0.72}$, while the full (black) line corresponds to the prediction in Eq. (27). Similar results are obtained from $\rho_v \simeq \xi_2^{-2}$ (not shown).

6 Conclusions

This paper should contribute to the understanding of the dynamics of topological defects across classical thermal phase transitions.

The framework we focused on is one in which the system of interest is coupled to an environment in equilibrium at a given temperature. The contact to the bath induces dissipative stochastic dynamics that, for concreteness, we chose not to conserve the order parameter. The system is taken across a phase transition by either varying the temperature of the external bath or by tuning a parameter in its Hamiltonian. The disordered (high temperature) phase is plagued with topological defects. After entering the ordered (low temperature) phase the system's configuration is out of equilibrium and the system relaxes by changing their organization and reducing their density. The nature and structure of topological defects depends strongly on the dimension of the order parameter, n ,

and the dimension of space, d . For the scalar case, $n = 1$, the defects are domain walls and these are points in $d = 1$, lines in $d = 2$ and surfaces in $d = 3$. For $n = d$ the defects are point-like and the example at hand are vortices in $d = 2$. While the ordering kinetics of systems subjected to instantaneous quenches has been studied at length with field theoretical and numerical techniques [9], the analysis of the effect of infinitely slow cooling rates has not been developed to the same extent (see [10, 11, 12, 13]). The Kibble-Zurek mechanism – based on critical scaling above the critical point – provides a concrete prediction for the density of defects left over across a phase transition when this is crossed at very low rate. This proposal captures correctly the moment and parameter value at which the system falls out of equilibrium (see [13] for a very detailed calculation in the 1d Glauber Ising chain) but neglects, incorrectly in dissipative thermal phase transition, the relaxation dynamics in the ordered phase. In [20] the case of a second-order phase transition with discrete spontaneously broken symmetry was discussed. In this paper we studied a different type of transition, the BKT one in the 2d XY model.

To summarize our results, we first analyzed in more detail than previously done the out of equilibrium relaxation of a 2d XY model infinitely rapidly quenched from $T_0 \rightarrow \infty$ to $T < T_{KT}$. Using MC simulations we confirmed the functional form of the growth law $\xi(T, t) \simeq [\lambda(T)t/\ln t/t_0]^{1/2}$ derived in [32, 33] and we determined its temperature dependence numerically. Although the log-correction has a theoretic foundation, this law has been frequently confused with an effective power law, especially in the field of freely decaying 2d turbulence as modelled with a Ginzburg-Landau approach [44]. We also analyzed the evolution of the structural properties such as the distribution of pair distances or the polarity correlation function in the course of time and we found that they all satisfy dynamic scaling with respect to the same growing length. Importantly enough, we demonstrated that the out of equilibrium dynamic properties are determined by the density of free vortices in the low- T phase as opposed to the density of all vortices that includes the equilibrium contribution of bound pairs. This fact is the reason for the failure of dynamic scaling when the length determined from the decay of the total density of vortices was used [46, 47]. Next, we studied cooling rate dependencies, we proposed a scaling form for the growing length under these circumstances, and we checked it numerically. We found that the density of free topological defects not only depends on the cooling rate used but does also on the time spent in the low temperature phase, where vortices and anti-vortices tend to bind or annihilate. In particular, the density of vortices at $t \simeq \tau_Q$ is $\rho_v \simeq [\tau_Q/\ln \tau_Q]^{-1}$ for very long τ_Q . In short, the dynamics in the critical low- T phase of the 2d XY is crucial to determine the density of topological defects.

Acknowledgements: This research was financially supported by ANR-BLAN-0346 (FAMOUS), in part by the National Science Foundation under Grant No. NSF PHY05-51164, and in part by the Swiss National Science Founda-

tion (SNSF). We thank very useful discussions with G. Biroli, P. Calabrese, D. Domínguez, G. Lozano, R. Rivers, and A. Sicilia.

References

- [1] A. N. Pargellis, S. Green, and B. Yurke, Phys. Rev. B **43**, 3699 (1991). I. Dierking, *Textures of Liquid Crystals* (Wiley-VCH, Weinheim, 2003).
- [2] C. Kawabat and A. R. Bishop, Solid State Comm. **60**, 167 (1986). H-J Elmers, J. Hauschild, G. H. Liu, and U. Gradmann, J. App. Phys. **79**, 4984 (1996). *Ultrathin magnetic structures*, ed. by J. A. C. Bland and B. Heinrich (Springer, Berlin, 1994). Int. J. Mod. Phys. B **9**, 3115 (1995).
- [3] A. Vilenkin and E. P. S. Shellard, *Cosmic Strings and other Topological Defects*, 2nd ed. (Cambridge University Press, Cambridge, 2000).
- [4] P. Tabeling, Phys. Rep. **362**, 1 (2002).
- [5] D. J. Bishop and J. D. Reppy, Phys. Rev. B **22**, 5171 (1980).
- [6] M. R. Beasley, Phys. Rev. Lett. **41**, 1165 (1979). A. F. Hebard and A. T. Fiory, Phys. Rev. Lett. **44**, 291 (1980).
- [7] A. N. Pargellis, S. Green, and B. Yurke, Phys. Rev. E **49**, 4250 (1994).
- [8] Y. S. Karimov and Y. N. Novikov, Zh. Eksp. Teor. Fiz. Pis'ma Red. **19**, 268 (1974); Sov. Phys. - JETP Lett. **19**, 159 (1974). D. J. Bishop and J. D. Reppy, Phys. Rev. Lett. **40**, 1727 (1978).
- [9] A. J. Bray, Adv. in Phys. **43**, 357 (1994). Puri, Phase trans. L. F. Cugliandolo, Physica A
- [10] S. Cornell, K. Kaski, and R. Stinchcombe, Phys. Rev. B **45**, 2725 (1992). S. Suzuki, J. Stat. Mech. P03032 (2009).
- [11] D. A. Huse and D. S. Fisher, Phys. Rev. Lett. **57**, 2203 (1986).
- [12] H. Yoshino, K. Hukushima, H. Takayama Phys. Rev. B **66**, 064431 (2002).
- [13] P. Krapivsky, J. Stat. Mech. P02014 (2010).
- [14] T. W. B. Kibble, J. Phys. A **9**, 1387 (1976).
- [15] W. H. Zurek, Nature (London) **317**, 505 (1985); Phys. Rep. **276**, 177 (1996).
- [16] V. M. H. Ruutu, V. B. Eltsov, A. J. Gill, T. W. B. Kibble, M. Krusius, Y. G. Makhlin, B. Placais, G. E. Volovik, W. Xu, Nature **382**, 334 (1996). C. Bäuerle, Y. M. Bunkov, S. N. Fisher, H. Godfrin, G. R. Pickett, Nature **382**, 332 (1996). The Grenoble cosmological experiment: the Kibble-Zurek

- scenario in superfluid ^3He , C. Bauerle, Yu. M. Bunkov, S. Fisher, and H. Godfrin, in *Topological defects and the non-equilibrium dynamics of symmetry breaking phase transitions*, Vol 549, Y. M. Bunkov and H. Godfrin eds. (Kluwer Academic Publishers, 1999).
- [17] G. Karra and R. J. Rivers, *Phys. Rev. Lett.* **81**, 3707 (1998). R. J. Rivers, *Phys. Rev. Lett.* **84**, 1248 (2000).
 - [18] P. Laguna and W. H. Zurek, *Phys. Rev. Lett.* **78**, 25 19 (1997); *Phys. Rev. D* **58**, 5021 (1998). A. Yates and W. H. Zurek, *Phys. Rev. Lett.* **80**, 5477 (1998). N. D. Antunes, L. M. A. Bettencourt, W. H. Zurek, *Phys. Rev. Lett.* **82**, 2824 (1999).
 - [19] T. W. B. Kibble, *Phys. Today*, **60**, 47 (2007).
 - [20] G. Biroli, L. F. Cugliandolo, and A. Sicilia, *Phys. Rev. E* **81**, 050101 (2010).
 - [21] N. D. Antunes, P. Gandra, and R. J. Rivers, *Phys. Rev. D* **73**, 125003 (2006).
 - [22] W. H. Zurek, U. Dorner, P. Zoller, *Phys. Rev. Lett.* **95**, 105701 (2005).
 - [23] A. Polkovnikov, *Phys. Rev. B* **72**, 161201 (2005).
 - [24] J. Dziarmaga, *Phys. Rev. Lett.* **95**, 245701 (2005). *Adv. in Phys.* **59**, 1063 (2010).
 - [25] T. Caneva, R. Fazio, and G. E. Santoro, *Phys. Rev. B* **76**, 144427 (2007). F. Pellegrini, S. Montangero, G. E. Santoro, and R. Fazio, *Phys. Rev. B* **77**, 140404 (2008). E. Canovi, D. Rossini, R. Fazio, G. E. Santoro, *J. Stat. Mech.* P03038 (2009).
 - [26] U. Divakaran, V. Mukherjee, A. Dutta A, and D. Sen, *J. Stat. Mech.* P02007 (2009). S. Mondal, K. Sengupta, D. Sen, *Phys. Rev. B* **79**, 045128 (2009).
 - [27] A. Polkovnikov, K. Sengupta, A. Silva, M. Vengalattore, arXiv:1007.5331.
 - [28] V. L. Berezinskii, *Zh. Eksp. Teor. Fiz.* **59**, 907 (1970) [*Sov. Phys. JETP* **32**, 493 (1971)].
 - [29] J. M. Kosterlitz and D. J. Thouless, *J. Phys. C* **6**, 1181 (1973). J. M. Kosterlitz, *J. Phys. C* **7**, 1046 (1974).
 - [30] H-C Chu and G. A. Williams, *Phys. Rev. Lett.* **86**, 2585 (2001).
 - [31] M. Hasenbusch, *J. Phys. A* **38**, 5869 (2005). M. Hasenbusch, A. Pelissetto, E. Vicari, *J. Stat. Mech.* P12002 (2005).
 - [32] B. Yurke, A. N. Pargellis, T. Kovacs, and D. A. Huse, *Phys. Rev. E* **47**, 1525 (1993).

- [33] A. J. Bray and A. D. Rutenberg, Phys. Rev. E **49**, R27 (1994). A. D. Rutenberg and A. J. Bray, *ibid* **51**, 5499 (1995).
- [34] U. Wolff, Nucl. Phys. B **322**, 759 (1989).
- [35] R. Gupta and C. F. Baillie, Phys. Rev. B **45**, 2883 (1992).
- [36] H. J. Luo and B. Zheng, Mod. Phys. Lett. B **11**, 615 (1997). B. Zheng, M. Schulz, and S. Trimper, Phys. Rev. E **59**, R1351 (1999).
- [37] H. J. Luo, M. Schulz, L. Schulke, S. Trimper, and B. Zheng, Phys. Lett. A **250**, 383 (1998).
- [38] Y. Ozeki, K. Ogawa, and N. Ito, Phys. Rev. E **67**, 026702 (2003).
- [39] S. T. Bramwell and P. C. W. Holdsworth, J. Phys.: Cond. Matt. **5**, L53 (1993); Phys. Rev. B **49**, 8811 (1994).
- [40] T. Nagaya, H. Hotta, H. Orihara, and Y. Ishibashi, J. Phys. Soc. Jpn. **61**, 3511 (1992). T. Nagaya, H. Orihara and Y. Ishibashi, *ibid* **64**, 78 (1995).
- [41] L. F. Cugliandolo, J. Kurchan, and G. Parisi, J. Phys. I (France) **4**, 1641 (1994).
- [42] L. Berthier, P. W. C. Holdsworth, and M. Sellitto, J. Phys. A **34**, 1805 (2001).
- [43] M. Mondello and N. Goldenfeld, Phys. Rev. A **42**, 5865 (1990).
- [44] G. Huber and P. Alström, Physica A **195**, 448 (1993).
- [45] A. J. Bray, A. J. Briant, and D. K. Jervis, Phys. Rev. Lett. **84**, 1503 (2000). A. J. Bray, **62**, 103 (2000).
- [46] F. Rojas and A. D. Rutenberg, Phys. Rev. E **60**, 212 (1999).
- [47] J-R Lee, S. J. Lee, and B. Kim, Phys. Rev. E **52**, 1550 (1995).
- [48] A. Jonsson and P. Minnhagen, Phys. Rev. B **55**, 9035 (1997).
- [49] D. Golubchik, E. Polturak, and G. Koren, arXiv:0911.5613.
- [50] F. Liu and G. F. Mazenko, Phys. Rev. B **46**, 5963 (1992).
- [51] D. A. Dimitrov and G. M. Wysin, J. Phys: Condens. Matt. **10** 7453 (1998).
- [52] J. J. Arenzon, A. J. Bray, L. F. Cugliandolo, and A. Sicilia, Phys. Rev. Lett. **98**, 145701 (2007). A. Sicilia, J. J. Arenzon, A. J. Bray, and L. F. Cugliandolo Phys. Rev. E **76**, 061116 (2007). A. Sicilia, Y. Sarrazin, J. J. Arenzon, A. J. Bray, and L. F. Cugliandolo, Phys. Rev. E **80**, 031121 (2009).
- [53] V. Ambegaokar, B. I. Halperin, D. R. Nelson, and E. D. Siggia, Phys. Rev. B **21**, 1806 (1980).